Journal of Hydrology 561 (2018) 494–508

Contents lists available at ScienceDirect

Journal of Hydrology

journal homepage: www.elsevier.com/locate/jhydrol

Research papers

Evaluating the hydraulic and transport properties of peat soil using pore network modeling and X-ray micro computed tomography

Behrad Gharedaghloo[a,*], Jonathan S. Price[a], Fereidoun Rezanezhad[b], William L. Quinton[c]

[a] Department of Geography and Environmental Management, University of Waterloo, Waterloo N2L 3G1, Canada
[b] Ecohydrology Research Group, Water Institute and Department of Earth and Environmental Sciences, University of Waterloo, Waterloo, Canada
[c] Cold Regions Research Centre, Wilfrid Laurier University, Waterloo, Canada

ARTICLE INFO

This manuscript was handled by C. Corradini, Editor-in-Chief, with the assistance of Masaki Hayashi, Associate Editor

Keywords:
Pore network modeling
Micro computed tomography
Imaging
Peat soil
Tortuosity
Solute transport

ABSTRACT

Micro-scale properties of peat pore space and their influence on hydraulic and transport properties of peat soils have been given little attention so far. Characterizing the variation of these properties in a peat profile can increase our knowledge on the processes controlling contaminant transport through peatlands. As opposed to the common macro-scale (or bulk) representation of groundwater flow and transport processes, a pore network model (PNM) simulates flow and transport processes within individual pores. Here, a pore network modeling code capable of simulating advective and diffusive transport processes through a 3D unstructured pore network was developed; its predictive performance was evaluated by comparing its results to empirical values and to the results of computational fluid dynamics (CFD) simulations. This is the first time that peat pore networks have been extracted from X-ray micro-computed tomography (μCT) images of peat deposits and peat pore characteristics evaluated in a 3D approach. Water flow and solute transport were modeled in the unstructured pore networks mapped directly from μCT images. The modeling results were processed to determine the bulk properties of peat deposits. Results portray the commonly observed decrease in hydraulic conductivity with depth, which was attributed to the reduction of pore radius and increase in pore tortuosity. The increase in pore tortuosity with depth was associated with more decomposed peat soil and decreasing pore coordination number with depth, which extended the flow path of fluid particles. Results also revealed that hydraulic conductivity is isotropic locally, but becomes anisotropic after upscaling to core-scale; this suggests the anisotropy of peat hydraulic conductivity observed in core-scale and field-scale is due to the strong heterogeneity in the vertical dimension that is imposed by the layered structure of peat soils. Transport simulations revealed that for a given solute, the effective diffusion coefficient decreases with depth due to the corresponding increase of diffusional tortuosity. Longitudinal dispersivity of peat also was computed by analyzing advective-dominant transport simulations that showed peat dispersivity is similar to the empirical values reported in the same peat soil; it is not sensitive to soil depth and does not vary much along the soil profile.

1. Introduction

In recent years, researchers have shown an interest in studying the transport of nutrient and solutes through peatlands. Several core-scale studies (Hoag and Price, 1997; Ours et al., 1997; Quinton et al., 2008; Boudreau et al., 2009; Rezanezhad et al., 2012) and field-scale studies (Hoag and Price, 1995; Baird and Gaffney, 2000; McCarter and Price, 2017a,b) have been done to characterize the hydraulic and transport properties of peat. The properties of porous materials are controlled by micro-scale pore distribution and pore topology (Vogel, 2002). However, little attention has been paid to the link between water flow and transport properties in peat, and the role of its pore characteristics. Quinton et al. (2008, 2009) and Rezanezhad et al. (2009, 2010) studied the relationship between peat hydraulic properties and its pore characteristics using images captured by camera or by X-ray micro computed tomography (μCT). These studies calculated pore conductance and pore hydraulic radius on 2D images. However, no studies have fully coupled the solute transport properties of peat soils and their relationship with micro-scale pore properties such as tortuosity and pore radius.

Pore network models (PNMs), despite having limitations, have helped to increase our understanding of multiphase flow (Vogel and Roth, 1998; Blunt, 2001; Nordhaug et al., 2003; Valvatne and Blunt, 2004; Dong and Blunt, 2009; Aghaei and Piri, 2015; Sheng and

* Corresponding author.
E-mail addresses: bghareda@uwaterloo.ca (B. Gharedaghloo), jsprice@uwaterloo.ca (J.S. Price), frezanez@uwaterloo.ca (F. Rezanezhad), wquinton@wlu.ca (W.L. Quinton).

https://doi.org/10.1016/j.jhydrol.2018.04.007
Received 13 September 2017; Received in revised form 1 April 2018; Accepted 2 April 2018
Available online 04 April 2018

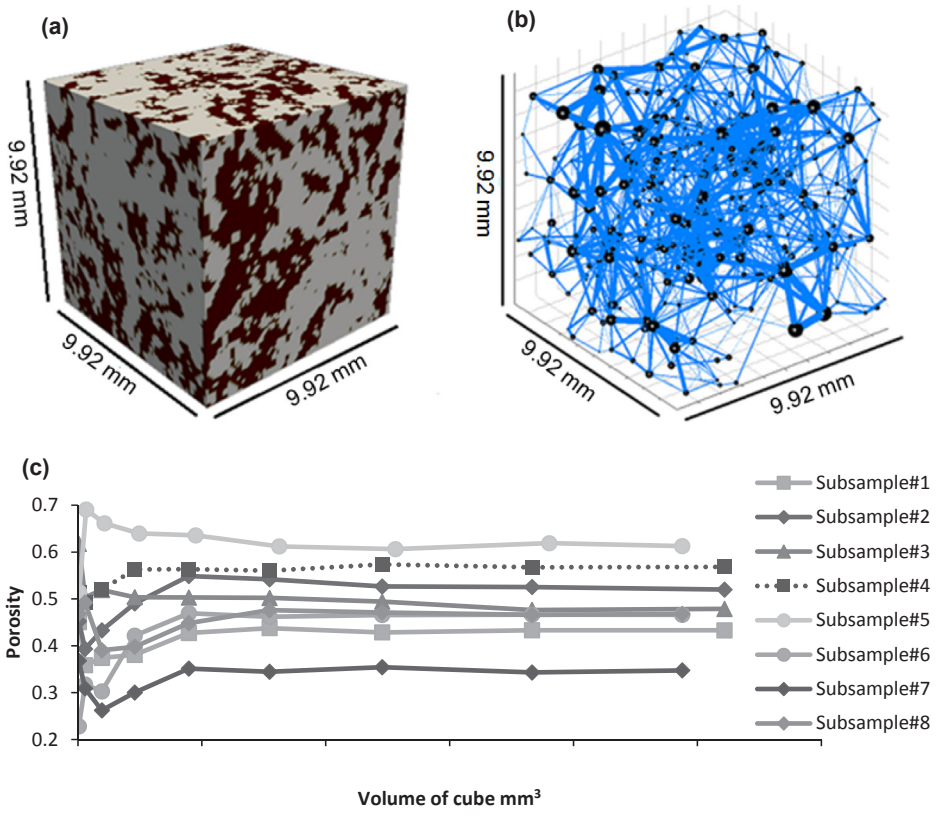

Fig. 1. (a) 9.92 × 9.92 × 9.92 mm (976 mm^3) X-ray μCT imaging data for peat soil at 2 cm depth; dark and light colors represent matrix and pore space, respectively. (b) Equivalent unstructured PNM from network extraction code; black spheres represent pore bodies (nodes) and cylinders are pore throats (bonds). (c) Examples of the variation of cube porosity versus cube volume on μCT images; the curves show that cube size used in this study is comparable to the REV of peat.

Thompson, 2016) and solute transport properties (Suchomel et al., 1998a; Meyers and Liapis, 1999; Bijeljic et al., 2004; Acharya et al., 2005, 2007; Bijeljic and Blunt, 2007; Raoof et al., 2013) of porous material. PNMs analyze pore morphological properties such as tortuosity (Sharratt and Mann, 1987; Armatas and Pomonis, 2004; Armatas, 2006), and can be used to characterize the relationship between pore topology and the resultant hydraulic properties of a porous media (Vogel and Roth, 2001; Arns et al., 2004). PNMs operate at a scale that can account for microscopic processes, such as the influence of a biomass accumulation and bio-clogging on permeability, in which the hydraulic properties of the medium are changing in response to flow through them (Thullner and Baveye, 2008; Ezeuko et al., 2011). Parameterizing at this scale and resolution is not practical or possible in field or even core-scale studies, especially of highly deformable *Sphagnum* dominated peat soils, while evaluating larger soil samples of peat masks the systematic reduction of peat hydraulic conductivity with depth. Therefore, PNMs provide an opportunity to better understand how peat structure, genesis, and state of decomposition affect flow and solute transport, in a detail not available through time-consuming laboratory experiments. However, it should be noted that simulation of flow and transport through 3D networks at sample sizes typical of laboratory measurements are computationally intensive.

There have been different approaches for constructing PNMs for a porous medium to represent its pore space. Previous researchers have used structured 2D (Suchomel et al., 1998b; Chen-Charpentier, 1999; Yiotis et al., 2001; Ezeuko et al., 2011) or structured 3D networks (Meyers and Liapis, 1998; Vogel, 2000; Li et al., 2006; Thullner and Baveye, 2008). A number of studies constructed PNMs using random functions obtained from μCT imaging data (Raoof et al., 2010; Köhne et al., 2011). Few studies extracted physically realistic disordered 3D PNMs through direct mapping the μCT imaging data (Al-Raoush and Willson, 2005; Silin and Patzek, 2006; Al-Kharusi and Blunt, 2007). Dong and Blunt (2009) developed a network extraction code that processes the μCT images to quantify the spatial distribution and geometry of pore bodies and pore throats, and their state of connectivity. They simulated multiphase flow through the extracted pore networks and observed good agreement between simulation results and empirical data. Over decades, solute transport studies in PNMs have been studied on 3D regular networks (e.g. Acharya et al., 2005, 2007; Li et al., 2006; Raoof et al., 2010) and on irregular networks which are extracted by direct mapping of the pore space (Kim et al., 2011; Mehmani and Balhoff, 2015; Mehmani et al., 2014; Mehmani and Tchelepi, 2017). The goal of this study is to gain a better understanding of flow and transport processes in peat soils by simulating flow and transport processes through the 3D pore networks extracted through direct mapping the pore space in X-ray μCT images of peat deposits. The specific objectives are to (1) evaluate the characteristics of pore structure in a 3D approach for peat deposits, (2) calculate peat hydraulic properties including horizontal (K_h) and vertical (K_v) hydraulic conductivities and pore tortuosity (τ) by simulating water flow, and examine how they change with depth (hence state of peat decomposition), and (3) determine bulk solute transport properties such as hydrodynamic dispersion, longitudinal dispersivity (α_L) and effective diffusion coefficient (D_{eff}), which are used in conventional numerical modeling, by simulating the convective/diffusive solute transport in peat pore spaces. The results help us to fundamentally answer how the variations of peat pore characteristics can influence the flow and transport properties of peat deposits. Also, since some of the parameters such as tortuosity and effective diffusion coefficient and their vertical heterogeneity along the soil profile are difficult to characterize in the laboratory, the calculated values can be used as inputs for core-scale or field-scale continuum models.

2. Methods and model development

Unstructured PNMs were extracted using a pore network extraction code developed by Dong and Blunt (2009). X-ray μCT data of *Sphagnum* peat soil at different depths (see Rezanezhad et al., 2009, 2010) were used as the input data for the network extraction code, which generated the spatial distribution and geometries of pore bodies and pore throats

including the shape, length, radius, volume and state of their interconnectivity. Fig. 1 illustrates an example of the raw 3D X-ray μCT data that was imported to the network extraction code (a), and the extracted PNM representing peat pore space (b). The size of voxels in the μCT data was 112.7 μm, with 88 voxels along the sides of the μCT cubes, leading to a dimension of ~1 cm^3 for each cube. Voxels of this size capture pores with radii ~ 100 μm. The majority of the interconnected macro-pores in peat, which control the bulk transport of water and solute and determine the macroscopic properties including hydraulic conductivity and dispersivity, have radii larger than 100 μm. To explore if this sample volume adequately characterizes the peat, a representative elementary volume (REV) analysis was done on eight subsamples (Fig. 1c); it showed the cubes sufficiently exceeded the REV of porosity, thus can represent the porosity of the peat samples. However, the REV of permeability could be larger than that of porosity (Mostaghimi et al., 2013; Berg et al., 2016). Based on the work of Mostaghimi et al. (2013), the ratio of "flow-based" REV to porosity-based REV can be up to 2. Considering the cubes used here are more than twice the size of porosity REV, cubes are likely of similar dimension to the "flow-based" REV representing permeability and dispersivity. Details of the X-ray μCT and image processing procedures are available in Rezanezhad et al. (2009, 2010). In this study, the saturated water flow and unsteady-state solute transport processes were simulated for the extracted PNMs using the model developed herein.

The primary application of this model is to simulate saturated water flow and unsteady state solute transport through unstructured PNMs. The first module of the model simulates saturated water flow through PNMs. Water flow through a pore throat can be expressed as

$$Q_{th} = g_p\left(\frac{\Phi_{Upgradient\ pore\ body} - \Phi_{Downgradient\ pore\ body}}{l}\right) \quad (1)$$

where Q_{th} [L^3T^{-1}] is the rate of water flow through the pore throat, g_p is pore flow conductance [L^5TM^{-1}] calculated based on the criteria discussed in Valvatne and Blunt (2004), $\Phi_{Upgradient\ pore\ body}$ and $\Phi_{Downgradient\ pore\ body}$ [$ML^{-1}T^{-2}$] are water pressure in the upgradient and downgradient pore bodies, respectively, and l is the pore length [L].

The sum of water flow into a pore body equals the sum of pore throat flow rates discharging from it, giving a linear water balance equation for each pore body. Water balance equations of all pore bodies form a system of linear equations that is solved implicitly to calculate water pressure in the pore bodies (e.g. Blunt and King, 1991; Oren et al., 1998; Valvatne and Blunt, 2004). Once the pore body pressures are determined (e.g. Fig. 2), Eq. (1) is used to calculate the water flow rate in pore throats. Next, the equivalent hydraulic conductivity of the PNM is calculated using the bulk water flow rate, dimensions of the network and Darcy's law. The details on the methods used here to simulate saturated water flow in PNMs are available in Valvatne and Blunt (2004) and in (Fig. 3).

The second module of the developed code simulates advective and diffusive mass fluxes along PNMs, and calculates the concentration in pore-bodies and pore-throats during simulation. The sets of formulae for solute transport simulations are obtained from Raoof et al. (2013) and Qin and Hassanizadeh (2015); here, the formulae in those papers are reduced to the transport of a conservative tracer in the absence of chemical reactions. The final pore body and pore throat equations are Eqs. (3) and (2), respectively, which are solved iteratively (details in Fig. 3) to obtain the temporal variations of solute concentration in all the pore elements. Fig. 4 illustrates examples of solute concentration in pore bodies after a 1.5 pore volume injection, in solute transport simulations. Derivations of Eqs. (3) and (2) and definitions of their parameters are briefly included in Appendix A. Qin and Hassanizadeh (2015) provided more details on deriving and solving these equations.

$$C_{ij}^{t+\Delta t} = C_i^{t+\Delta t}\frac{(N_{ij}\max(Q_{ij},0) + N_{ij}B_{ij})}{(1 + N_{ij}|Q_{ij}| + 2N_{ij}B_{ij})} - C_j^{t+\Delta t}\frac{(N_{ij}\min(Q_{ij},0) - N_{ij}B_{ij})}{(1 + N_{ij}|Q_{ij}| + 2N_{ij}B_{ij})} + \frac{C_{ij}^t}{(1 + N_{ij}|Q_{ij}| + 2N_{ij}B_{ij})} \quad (2)$$

$$C_i^{t+\Delta t}\left(1 + M_i\sum_j \max(Q_{ij},0) + M_i\sum_j B_{ij} - M_i\sum_j \frac{N_{ij}B_{ij}(|Q_{ij}| + B_{ij})}{(1 + N_{ij}|Q_{ij}| + 2N_{ij}B_{ij})}\right) = \left[M_i\sum_j N_{ij}\frac{(B_{ij} - \min(Q_{ij},0))^2}{(1 + N_{ij}|Q_{ij}| + 2N_{ij}B_{ij})}C_j^{t+\Delta t}\right] + M_i\sum_j \frac{(B_{ij} - \min(Q_{ij},0))C_{ij}^t}{(1 + N_{ij}|Q_{ij}| + 2N_{ij}B_{ij})} + C_i^t \quad (3)$$

The mixed cell method (MCM), which assumes a perfect mixing in pore bodies during solute transport simulation, is used here. For the media in which the mixing in the pore bodies is not perfect, MCM causes significant errors during pore network modeling of advective transport (Mehmani et al., 2014). Besides, the implementation of flow and transport equations, representation of pore space by a PNM, and numerical approximation of transport equations might introduce errors in the simulation results. Therefore, the results of the simulation code need to be evaluated against direct numerical simulation (DNS) results and empirical values. Details of the methods and the results of the evaluations are in Appendix B. The evaluation results showed a good match between DNS and PNM results. Mehmani et al. (2014) observed that the error imposed to the model's predictions due to the perfect mixing assumption is negligible in unstructured granular media. Since the pore space of peat is more unstructured than that of granular media, it is not surprising to observe similarity of DNS and PNM results, and that the assumption of perfect mixing hasn't introduced significant errors in PNM predictions. In addition, there was good agreement between PNM predictions and empirical values; all these demonstrate good predictive performance of the simulation code. It must be noted that the validity of the PNM results in this study does not justify the validity of perfect mixing in all porous media. When simulating solute transport in the PNMs of other media, DNS and PNM results must be compared to observe the quality of agreement between them and to assess the level of error imposed by simplifying assumptions of PNMs.

Nine cubes of 3D μCT data with dimensions of 9.92 mm × 9.92 mm × 9.92 mm were selected from different depths of *Sphagnum* peat X-ray μCT data. PNM of each cube was extracted using the network extraction code of Dong and Blunt (2009). Raw simulation results, which are the spatial variations of pore body pressure and pore throat flow rates, and spatial and temporal variations of solute concentration along PNMs, were analyzed to calculate the bulk properties of peat (Fig. 3). Appendix C presents the details of the equation and algorithms used in post-processing to determine bulk properties of peat including hydraulic conductivity, effective diffusion coefficient, formation factor, hydrodynamic dispersion, longitudinal dispersivity, hydraulic tortuosity, and diffusional tortuosity. In a porous medium, hydraulic tortuosity is the ratio of actual flow length of fluid particles to the bulk length of the porous medium, and diffusional tortuosity is the ratio of actual travel length of solute species to the bulk length of the porous medium.

3. Results and discussion

For the peat samples used here to explore the PNM, the calculated saturated hydraulic conductivity (Table 1) was found to be high (~2.6×10^{-3} m.s^{-1}) at the near-surface layers where the poorly decomposed or living mosses cover the soil surface. Although the effective porosity declined 2.3 times, the hydraulic conductivity values declined 50 times in 10 cm of the surface peat profile, which suggests that there are reasons for the dramatic reduction of peat hydraulic conductivity

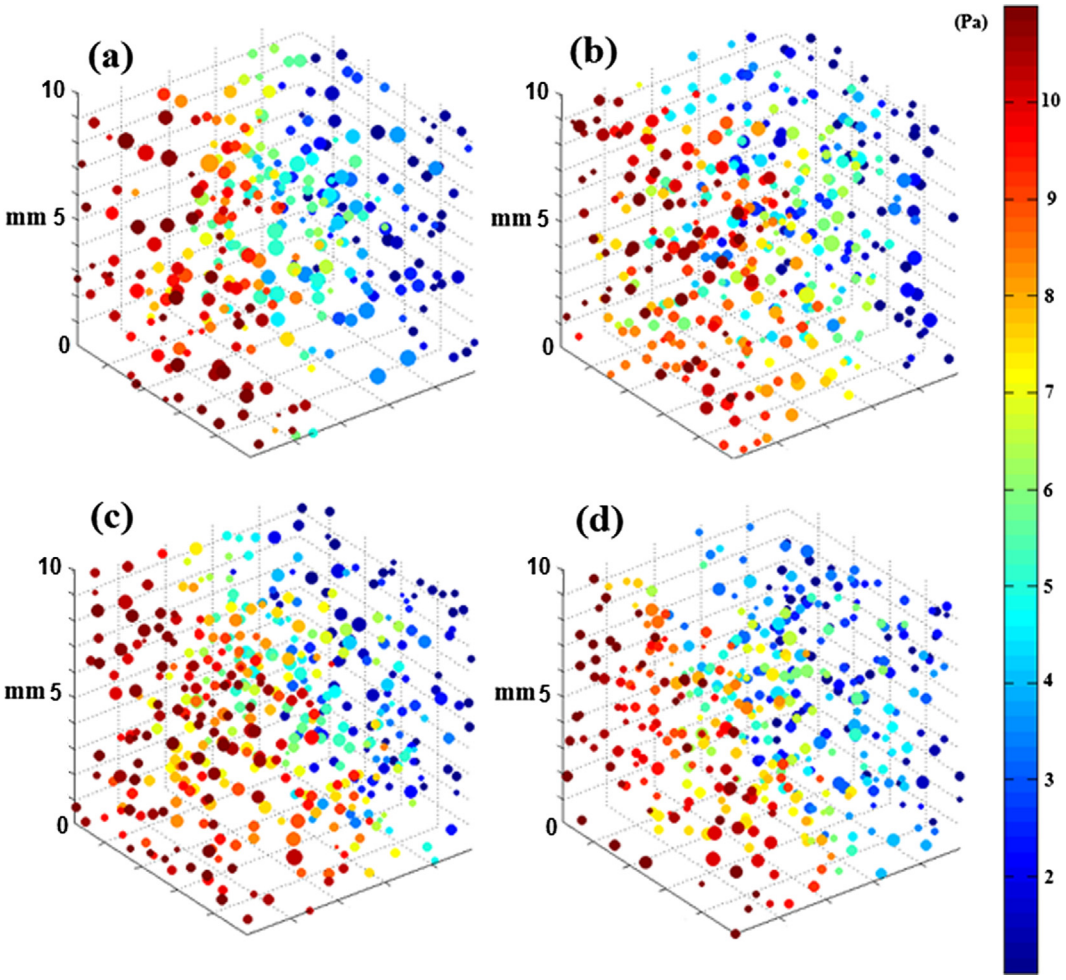

Fig. 2. Simulated pressure in pore bodies for peat soil located at (a) 2 cm, (b) 5 cm, (c) 9 cm, and (d) 10 cm depth, in which the upstream is the left face of each cube.

other than reduced effective porosity. The trend is similar to the sharp reduction of hydraulic conductivity with depth shown by Rezanezhad et al. (2010) on the same X-ray μCT data. A similar decline in peat hydraulic conductivity with depth has also been shown by other researchers (e.g., Boelter and Verry, 1977; Hoag and Price, 1995; Price et al., 2008). K_h at 9 cm depth was calculated to be 6.1×10^{-3} m.s^{-1}; the value is comparable to the empirical values reported by Quinton et al. (2008) for the same soil at the same depth (3.5×10^{-3} m.s^{-1} and 1.0×10^{-2} m.s^{-1}).

In this study, K_h and K_v were similar at a given depth (Table 1), illustrating isotropic hydraulic conductivity. Peat hydraulic conductivity is commonly reported to be anisotropic, with $K_h > K_v$ (Fraser et al., 2001; Kruse et al., 2008; Lewis et al., 2012). However, anisotropy in peat can be scale-dependent, and it is not surprising to see a lack of anisotropy at small scales (Beckwith et al., 2003). Upscaling the calculated K_h values with arithmetic averaging (since horizontal flow is parallel to peat horizons), and K_v by harmonic averaging (since vertical flow is perpendicular to peat horizons) (see Bear, 1972, p.151–154) results in average K_h and average K_v, respectively, as 1.1×10^{-2} and 4.5×10^{-3} m.s^{-1}, thus an anisotropy factor of ~2.4 for hydraulic conductivity in the peat profile. Thus, peat hydraulic conductivity can be isotropic at the micro-scale, but due to its systematic layering, wherein K_h exceeds K_v, hydraulic conductivity becomes anisotropic at the core- or field-scale. The distinct reduction of K_v with depth in the upper peat horizons highlights an important consideration in upscaling of K_v for shallow peat layers. If we calculate K_v at a given depth, e.g. at 6 cm, the average upward K_v is the weighted harmonic mean of K_v values observed from 6 cm to 2 cm depth. Similarly, downward K_v is the weighted harmonic mean of K_v values observed between 6 and 10 cm depth. The calculated upward up-scaled K_v and downward up-scaled K_v are 1.34×10^{-2} m.s^{-1} and 5.02×10^{-3} m.s^{-1} at 6 cm depth, respectively. The layered heterogeneity of peat soils and the sharply declining trend of K_v within a few centimeters lead to an apparent anisotropy of K_v that necessitates considering it in the simulation of water infiltration and solute transport through shallow peat horizons.

Decreasing peat hydraulic conductivity with depth can be due to the variations of peat pore radius with depth. The cumulative pore size distributions at 3 different depths (Fig. 5a) showed that the radii of the pores that form the pore volume of peat become smaller with increasing depth. The average pore body radius (R_{pore_body}) and pore throat radius (R_{pore_throat}) calculated for each PNM decreased with depth (Fig. 5b). The decrease in R_{pore_body} and R_{pore_throat} with depth explains the lower hydraulic conductivity there (Fig. 5c). The hydraulic conductivity of a porous medium is also inversely proportional to the tortuosity of the medium (Bear, 1972). To determine the hydraulic tortuosity, as shown in Fig. 3 and discussed in Appendix C, particle tracking was done on each PNM to obtain the distribution of particle's actual flow length in the network. Particle tracking results revealed that hydraulic tortuosity increases with depth (Table 1) where peat is more decomposed and has a higher bulk density (cf. Rezanezhad et al., 2010). Hydraulic tortuosity values obtained here are approximately half of the values reported by Rezanezhad et al. (2010), who estimated it as a fitting parameter, rather than directly. According to Carman (1937), increasing tortuosity reduces hydraulic conductivity. Thus, a combination of smaller pore-size and greater tortuosity with depth in a peat profile explains its lower hydraulic conductivity with depth. The average coordination number of

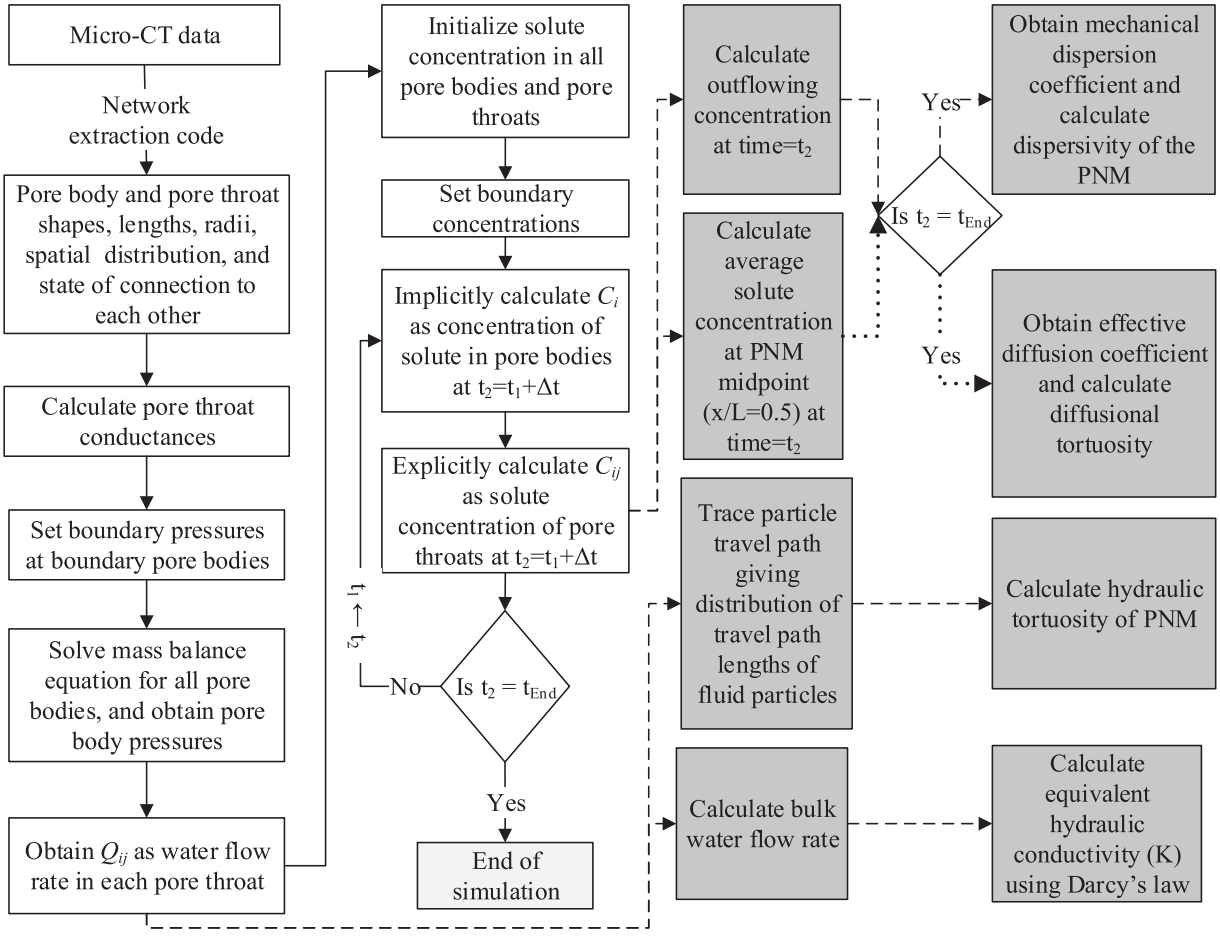

Fig. 3. Algorithm of model developed to simulate water flow and solute transport through pore networks and to calculate peat hydraulic and transport properties.

pore network, which is the average number of pore bodies that an individual pore body is connected to, decreased with increasing depth. This means that due to compaction and decomposition, the number of the connecting paths between pores decreases with depth. The reduction in average coordination number explains the increase of tortuosity with depth; as the number of pores connected to a pore body decreases, the possibility that fluid parcels travel along a straight path decreases, thus the parcel's path becomes more deviated and tortuous.

The ratio of the effective diffusion coefficient to the molecular diffusion coefficient (D_{eff}/D_m) decreased along the depth profile (Table 1) declining from 0.38 at 2 cm depth to 0.060 at 11 cm depth. This is due to the reduction in porosity and increased tortuosity down the peat profile. Similar to hydraulic tortuosity (τ_h), calculated diffusional tortuosity (τ_d) and electrical tortuosity (τ_e), which is analogous to diffusional tortuosity (see Appendix C), increased with respect to peat depth (Table 1). This suggests the migration path of the diffusing solute particles becomes more tortuous with increasing degree of decomposition. For all the pore networks, τ_d was smaller than τ_h. This has been observed and been reported frequently for other porous material (e.g., Zhang and Knackstedt, 1995; Saomoto and Katagiri, 2015). Diffusional pore conductance is proportional to pore radius to the power of two, while hydraulic pore conductance is proportional to pore radius to the power of four; this causes flow paths of fluid particles to become more tortuous and longer than it is for solute particles (Ghanbarian et al., 2013).

The formation factor of a porous medium (F) is a measure of the connectivity of pores in the medium based on their ability to conduct electrical current. F is determined as the ratio of the resistivity of medium when it is saturated with brine to the resistivity of the brine and is a function of porosity; F also is equal to D_m/D_{eff} (details provided in Appendix C). Comparing D_m/D_{eff} against peat porosity (using the data of Table 1) (and fitting Eq. (C.7) from Appendix C to the data), a and m –which are parameters relating F and D_m/D_{eff} to peat porosity and are defined in Appendix C– are calculated as 0.79 and 2.41, respectively, with R^2 of 0.98 (note: Quinton et al. (2008) also obtained m as 2.3 with a completely different methodology that fitted calculated hydraulic conductivity values on measured ones). It should be noted that m is a function of pore shape and specific surface area and increases as pores become irregularly shaped and as pore specific surface area rises (Salem, 2001). It also increases with increased compaction in porous material (Wyble, 1958). We know peat specific surface area increases as its average pore radius decreases with depth. Compaction of peat and the higher specific surface area in deep peat layers due to decomposition causes m to increase with depth. Larger m in deeper peat horizons leads to smaller D_{eff}, even if porosity is constant. In other words, the reduction of effective diffusion coefficient and diffusive mass flux due to increasing peat tortuosity likely is more intense in deep peat layers compared to that in near-surface horizons. This can significantly decrease the diffusion of nutrients from mineral layer beneath a peatland into the peatland. It also can prevent transport of contaminating solutes from the peat layer into the underlying mineral layer. In other word, deep highly decomposed peat layers might function as natural diffusion barriers in peatlands.

Longitudinal dispersion values were obtained by matching the simulated breakthrough curves with analytical solutions of the advection-dispersion-equation, and then the longitudinal dispersion and average pore velocities were used to calculate longitudinal dispersivity (details discussed in Appendix C). Dispersivity ranged from 2.19×10^{-3} m to 3.84×10^{-3} m (Table 1). Unfortunately, few studies have reported dispersion and dispersivity values for peat, and there is a

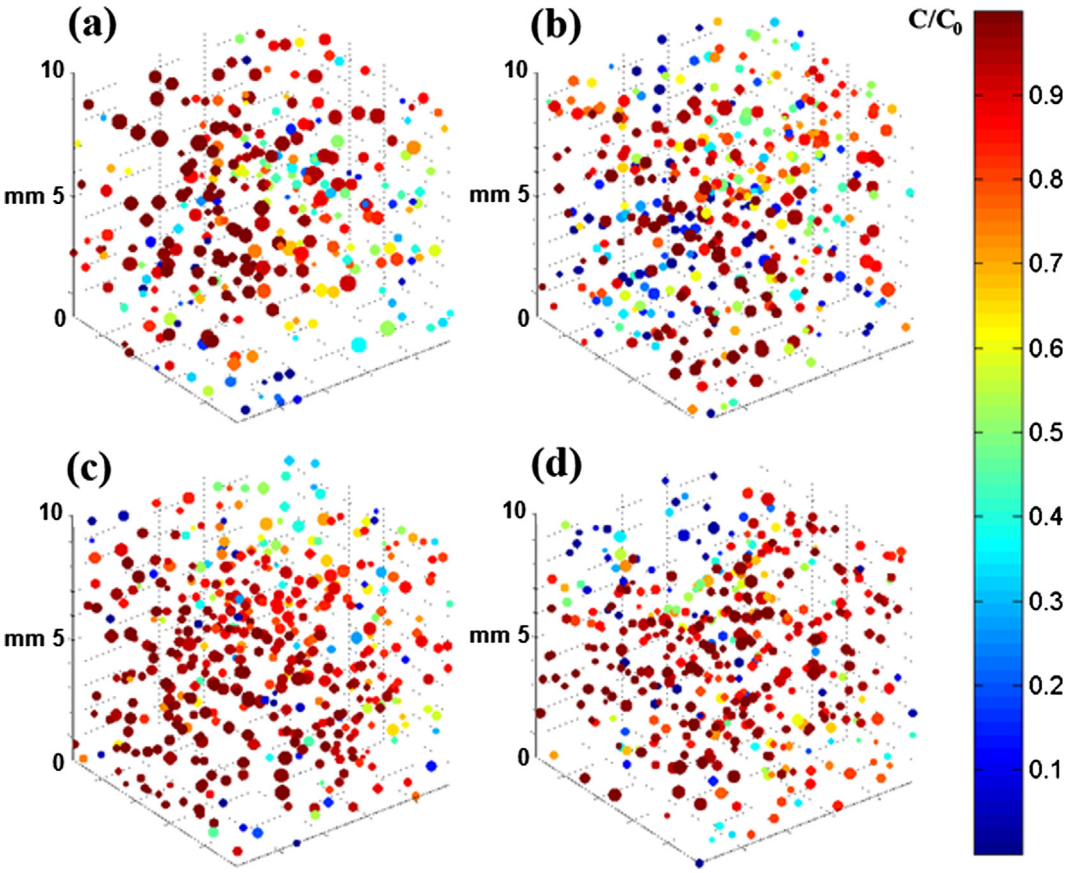

Fig. 4. Simulated solute concentration in pore bodies after 1.5 pore volume injection of solution into the pore network, obtained for peat located at (a) 2 cm, (b) 5 cm, (c) 9 cm, and (d) 10 cm depth.

gap of knowledge on how these parameters vary with peat depth and degree of decomposition. Hoag and Price (1997) measured chloride solute breakthrough curves for undisturbed peat cores obtained from a bog peatland and reported corresponding hydrodynamic dispersion values as well as average linear flow velocity. Their peat cores were extracted at 20 and 62 cm depth, and the dispersivity values were 1.6×10^{-3} m and 3.72×10^{-3} m, respectively. Our simulations resulted in similar values (Table 1). Ours et al. (1997) reported apparent dispersivity values equal to and larger than 4.0×10^{-3} m. However, Rosa and Larocque (2008) and Boudreau et al. (2009) reported dispersivity values an order of magnitude larger than the values obtained here. Dispersivity increases as porous media becomes more heterogeneous (Kantak et al., 1994). Klotz et al. (1980) observed that dispersivity in soil samples in laboratory tests increases as the variation of soil particle diameter increases. Increased variation of soil particle size leads to increased variations in pore radius. Variations of pore tortuosity and pore water velocity are directly related to dispersion and dispersivity (Fetter, 1999). It is therefore likely that the notable differences between dispersivity values observed here and in Hoag and Price (1997), with the values reported by Rosa and Larocque (2008) or Boudreau et al. (2009), are due to a large variation in pore tortuosity, or pore radius in their peat samples. Further studies are required to develop a better understanding of dispersivity in peat and its relationships with the type of peat, and its depth and degree of decomposition.

4. Conclusion

Simulation results with PMNs reproduced the dramatic decrease of hydraulic conductivity with respect to depth in the near-surface horizons of a peat profile that is commonly observed in field and laboratory studies (Hoag and Price, 1995, 1997; Rezanezhad et al., 2009, 2010). This is caused by a reduction of pore radius and an increase in tortuosity with depth. Diffusional tortuosity in peat, similar to other porous material, was found to be smaller than hydraulic tortuosity. Peat

Table 1
Number of pore bodies and pore throats and average pore coordination number in the extracted pore networks and the variation of active porosity (ε_a), simulated hydraulic conductivity, tortuosity (τ), dispersivity and D_{eff}/D_m values from 2 cm to 11 cm depth. These parameters are defined in Appendix C.

Depth (cm)	#Pore bodies	#Pore throats	Average pore coordination number	Active porosity (ε_a)	K_h (m.s^{-1})	K_v (m.s^{-1})	Hydraulic tortuosity τ_h	D_{eff}/D_m	Electrical and diffusional tortuosity τ_e, τ_d	Longitudinal dispersivity (α_L) (m)
2	311	1398	9.0	0.61	2.63×10^{-2}	2.50×10^{-2}	2.05	0.38	1.27	2.86×10^{-3}
3	312	1329	8.5	0.57	2.33×10^{-2}	2.23×10^{-2}	1.87	0.35	1.28	3.69×10^{-3}
5	490	1590	6.5	0.47	8.14×10^{-3}	9.00×10^{-3}	2.07	0.21	1.48	3.84×10^{-3}
6	406	1658	8.2	0.49	1.05×10^{-2}	1.14×10^{-2}	1.96	0.24	1.44	3.12×10^{-3}
9	452	1780	7.9	0.47	6.10×10^{-3}	5.80×10^{-3}	2.19	0.19	1.59	2.19×10^{-3}
10	433	1357	6.3	0.35	1.59×10^{-3}	1.56×10^{-3}	2.3	0.086	2	2.29×10^{-3}
11	469	1302	5.6	0.27	4.56×10^{-4}	4.52×10^{-4}	2.48	0.06	2.12	–

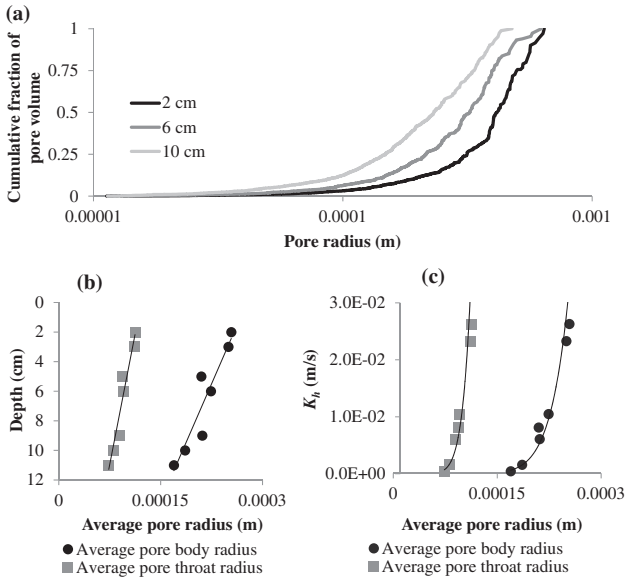

Fig. 5. (a) cumulative distributions of pore radii in different peat depths. (b) variation of peat average pore radius with depth. (c) variation of peat horizontal hydraulic conductivity with average pore radius.

dispersivity was determined through advection dominant transport PNM simulations, which showed that peat dispersivity does not vary considerably with depth. The values are in the same range of observed values for similar type of peat at similar depths (Hoag and Price, 1997; Ours et al. (1997). This study confirms that hydraulic properties of peat soils are controlled by their pore size and pore tortuosity.

Characterizing the effective diffusion coefficient of a porous medium by laboratory experiments is a time consuming process fraught with practical/technical difficulties, and conventional modeling of diffusion-dominant transport through peat soils requires an estimate of the effective diffusion coefficient. The PNM resulted the effective diffusion coefficient and its variation with depth through simulation of non-advective solute transport, illustrating that due to increasing tortuosity its decrease relative to pure molecular diffusion with depth. The effective diffusion coefficient of peat and its variation with depth received little attention in previous studies. Results suggested that the reduction in effective diffusion can be more intense in deeper peat horizons with higher states of decomposition.

Because of limitations in computational capabilities, network modeling is currently unable to simulate meso-scale or field-scale transport processes. However, based on small samples it can be used to extend fundamental knowledge on pore-scale phenomena, and to address how peat pore morphology controls the larger scale properties of peat. Furthermore, it can be used to characterize the systematic heterogeneities of pore morphology that cannot be physically measured.

Acknowledgements

We would like to thank Dr. Martin Blunt from Imperial College of London, UK who generously supplied the pore network extraction code. Research was funded by a NSERC Discovery Grant to Dr. Price.

Appendix A. Derivation of solute transport equations

The code solves the solute mass balance equations for the pore elements

$$V\frac{dC}{dt} = (QC)_{in} - (QC)_{out} - \left(D_m A\frac{dC}{dl_p}\right)_{in} + \left(D_m A\frac{dC}{dl_p}\right)_{out} \tag{A.1}$$

where V is the volume of a pore element (pore body or pore throat) [L^3], Q is the rate of water flowing into or out of the pore element [L^3T^{-1}], C is the solute concentration at the pore element [ML^{-3}], D_m is the molecular diffusion coefficient of solute [L^2T^{-1}], l_p is the length of pore element [L], and dC/dl_p is the concentration gradient along the pore element [ML^{-4}] which later is approximated as the gradient between a pore body (pore throat) and its adjacent pore throat (pore body). Applying Eq. (A.1) for pore throats and pore bodies (with considering multiple inlets/outlets in the pore bodies), Eqs. (2) and (A.3) are obtained for pore bodies and pore throats respectively, where i and j are the pore body indexes, and ij is the index of the pore throat that is connecting pore body i to pore body j.

$$V_i\frac{dC_i}{dt} = -C_i\sum_j \max(Q_{ij},0) - \sum_j C_{ij}\min(Q_{ij},0) - \sum_j D_{ij}A_{ij}\frac{C_i - C_{ij}}{L_{ij}/2} \tag{A.2}$$

$$V_{ij}\frac{dC_{ij}}{dt} = (C_i - C_{ij})\max(Q_{ij},0) + (C_{ij} - C_j)\min(Q_{ij},0) + D_{ij}A_{ij}\frac{(C_i - C_{ij})}{\left(\frac{L_{ij}}{2}\right)} + D_{ij}A_{ij}\frac{(C_j - C_{ij})}{\left(\frac{L_{ij}}{2}\right)} \tag{A.3}$$

Using an upwind scheme in approximating Eq. (A.2), Eq. (A.4), which is the numerically approximated form of solute transport equation in pore bodies, is obtained; M_i and B_{ij} are defined in Eqs. (A.5) and (A.6) respectively.

$$C_i^{t+\Delta t} = -M_i C_i^{t+\Delta t}\sum_j \max(Q_{ij},0) - M_i\sum_j C_{ij}^{t+\Delta t}\min(Q_{ij},0) - M_i\sum_j B_{ij}(C_i^{t+\Delta t} - C_{ij}^{t+\Delta t}) + C_i^t \tag{A.4}$$

$$M_i = \frac{\Delta t}{V_i} \tag{A.5}$$

$$B_{ij} = \frac{2D_{ij}A_{ij}}{L_{ij}} \tag{A.6}$$

Numerically approximating the Eq. (A.3) with upwind scheme and rearranging the obtained equation leads to Eq. (2), which is the final form of solute transport equation in pore throats; as defined in Eq. (A.7), N_{ij} is the ratio of time step size to the pore throat volume.

$$C_{ij}^{t+\Delta t} = C_i^{t+\Delta t}\frac{(N_{ij}\max(Q_{ij},0) + N_{ij}B_{ij})}{(1 + N_{ij}|Q_{ij}| + 2N_{ij}B_{ij})} - C_j^{t+\Delta t}\frac{(N_{ij}\min(Q_{ij},0) - N_{ij}B_{ij})}{(1 + N_{ij}|Q_{ij}| + 2N_{ij}B_{ij})} + \frac{C_{ij}^t}{(1 + N_{ij}|Q_{ij}| + 2N_{ij}B_{ij})} \tag{2}$$

$$N_{ij} = \frac{\Delta t}{V_{ij}} \tag{A.7}$$

Finally Eq. (3) is obtained by coupling Eqs. (2) and (A.4). Eqs. (2) and (3) are solved iteratively to calculate the temporal variations of solute concentrations in pore elements. The details of equations derivations and numerical solution procedure are presented in Qin and Hassanizadeh (2015).

$$C_i^{t+\Delta t}\left(1 + M_i \sum_j \max(Q_{ij},0) + M_i \sum_j B_{ij} - M_i \sum_j \frac{N_{ij}B_{ij}(|Q_{ij}| + B_{ij})}{(1 + N_{ij}|Q_{ij}| + 2N_{ij}B_{ij})}\right) = + \left[M_i \sum_j N_{ij} \frac{(B_{ij} - \min(Q_{ij},0))^2}{(1 + N_{ij}|Q_{ij}| + 2N_{ij}B_{ij})} C_j^{t+\Delta t}\right] + M_i \sum_j \frac{(B_{ij} - \min(Q_{ij},0)) C_{ij}^t}{(1 + N_{ij}|Q_{ij}| + 2N_{ij}B_{ij})} + C_i^t \tag{3}$$

Appendix B. Model evaluation

Flow and solute transport must first be validated by ensuring water and solute mass conservation. Water mass conservation in saturated flow simulations requires that the bulk rate of water flowing into the PNM equals the bulk rate of water flowing out. This is validated in the pore network simulation when the difference between the inflow and outflow rate is negligible (less than 0.001%). The conservation of solute mass in solute transport simulations needs

$$M_{injected}(t) = M_{produced}(t) + M_{accumulated} \tag{B.1}$$

where $M_{injected}$ is cumulative injected solute mass [M], $M_{produced}$ is cumulative produced (outflow) solute mass [M], and $M_{accumulated}$ is the mass of solute accumulated in the aqueous phase present in the pore network [M]. $M_{injected}$, $M_{produced}$, $M_{accumulated}$ were calculated as

$$M_{injected}(t) = Q_w \int_{t=0}^{t} C_0 dt = C_0 Q_w t \tag{B.2}$$

$$M_{produced}(t) = Q_w \int_{t=0}^{t} C_{outflow} dt \tag{B.3}$$

$$M_{accumulated}(t) = \sum_{i=1}^{N_{pore\ body}} C_i(t) V_i + \sum_{j=1}^{N_{pore\ throat}} C_j(t) V_j \tag{B.4}$$

where C_0 [ML^{-3}] is the source concentration, Q_w is the bulk water flow rate [L^3T^{-1}], and t is simulation time [T], $C_{outflow}$ [ML^{-3}] is the solute concentration at the outflow face of the pore network, C_i(t) is solute concentration at pore body i at time t, C_j(t) is solute concentration at pore throat j at time t, V_i is the volume of pore body i, V_j is the volume of pore throat j, $N_{pore\ body}$ is number of pore bodies in the pore network, and $N_{pore\ throat}$ is the number of pore throats in the pore network. Fig. B.1 illustrates an example of the aforementioned parameters in a solute transport simulation showing that Eq. (B.1) and consequently solute mass conservation are valid in the transport simulations.

The second step in validating the pore network modeling code was to compare its results to the results of direct numerical simulations (DNS) done using OpenFOAM, which is an open-source computational fluid dynamics (CFD) tool. An OpenFOAM model was constructed for each depth from the same X-ray μCT cube used for pore network extraction. First, the STereoLithography (STL) file of the surface representing the outer boundaries of the pore space in μCT images was exported using MICROVIEW (version 2.5.0-rc12). Next, a 3D mesh of the void space was constructed using blockMesh and snappyHexMesh, the meshing tools of OpenFOAM. Then, water flow and solute transport processes were simulated on the 3D mesh with boundary conditions and initial conditions identical to those used in the pore network simulations. For advective dominant simulations, the following steps are done: (1) A pressure gradient similar to that of pore network model is applied along the 3D mesh, and the Navier-Stokes equation is solved using icoFOAM solver of OpenFOAM, resulting in pressure and velocity variations along the 3D mesh; and (2) the simulated velocity vector is inserted as boundary condition and initial condition in transport simulations in which the initial concentration of solute in the 3D mesh is zero, the inflow boundary condition is a pulse injection of solute with a concentration of $C = C_0$ for half the simulation time and then $C = 0$ for the rest of simulation time (Fig. B.2); the outflow boundary condition is zero gradient. ScalarTransportFoam solver of OpenFOAM package is used to simulate concentration variations over time and space. For the diffusional cases, the elements of the velocity vector is considered zero (no advection) along the 3D mesh; initial solute concentration is $C = C_0$ along the 3D mesh, and boundary conditions at two end faces of the domain are $C = 0$. Eventually, post-processing of the simulation results, which are the variation of solute concentration in the 3D mesh with time, was done using

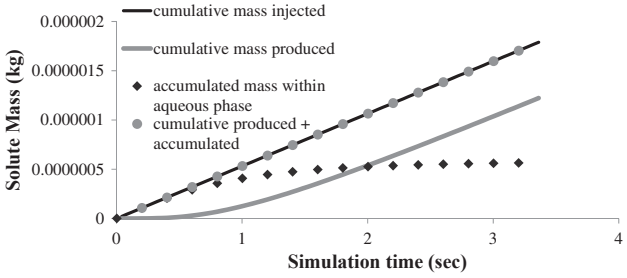

Fig. B.1. Example of solute mass balance in peat pore network solute transport simulations for the PNM at 2 cm depth; black line shows the variation of $M_{injected}$ with simulation time, grey line illustrates the variation of $M_{produced}$ over simulation time, black diamonds are $M_{accumulated}$ in the pore network over simulation time, and grey circles represent the sum of $M_{accumulated}$ and $M_{produced}$, which strongly matches the cumulative mass injected (black line), meaning that the solute mass balance error is negligible and solute mass conservation is valid along the simulation time.

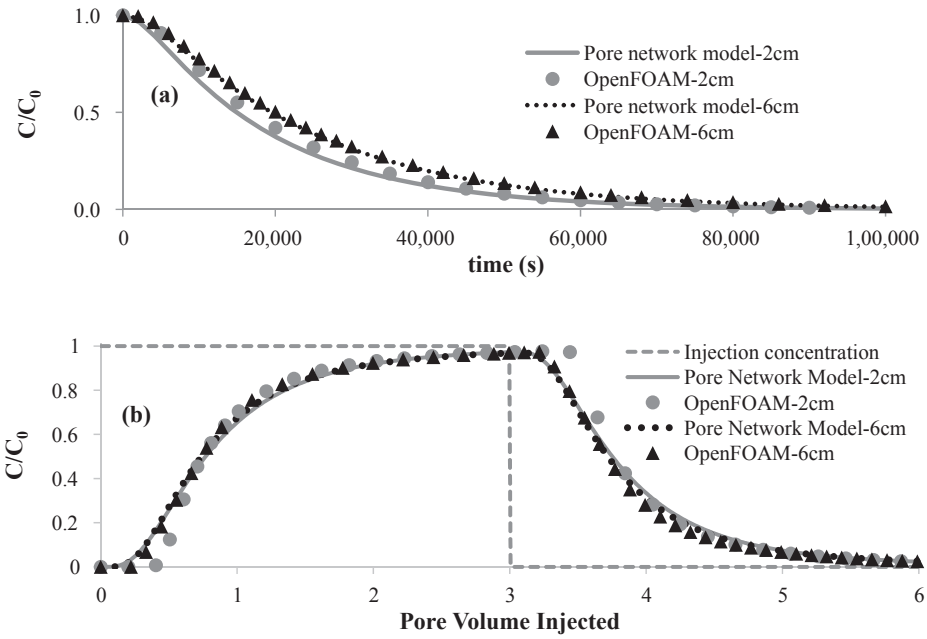

Fig. B.2. (a) Variation of solute concentration at $x = L/2$ of peat pore space in a diffusional transport process for peat at 2 and 6 cm depth, (b) variation of effluent solute concentration in an advective-dominant transport process, obtained by direct simulations with OpenFOAM, and by developed pore network modeling code for peat at 2 and 6 cm depth.

processing functions of PARAVIEW (Ahrens et al., 2005; Ayachit, 2015). In both diffusional transport simulations (Fig. B.2a) and advection-dominant transport simulations (Fig. B.2b), PNM results are in good agreement with DNS results. For sample of 6 cm depth, the matching quality in the declining part of the breakthrough curve (BTC) remained as good as the concentration rise part. For peat of 2 cm depth, mismatches are seen at the beginning of the rise and at the decline portion of the BTC; however, in the mid-concentrations and at the tails of the BTC matching quality is good. This early breakthrough might be due to a slight misrepresentation of the pore space by the network model; in direct mapping the pore space, a portion of the active pore volume might be assigned to pores bodies or pore throats that are not as actively transporting water (e.g. dead-end pores). Therefore, due to the underestimation of the active pore volume, which is transferring the advective flux, solute's arrival time is underestimated and the earlier breakthrough takes place at the outflow (Mehmani and Tchelepi, 2017). As the simulation time proceeds, the less-active pores contribute to the solute transport through diffusion which returns the BTC of PNM to the trend of the BTC of DNS.

The agreements between PNM and DNS results means the implementation of flow and transport equations in the pore network modeling code discussed in Section 2 and Appendix A has been done successfully. In addition, it shows the numerical approximation of the flow and transport equations, the approximation of pore spaces with the networks of pore bodies and pore throats, and the assumption of perfect mixing in the pore bodies impose little error on the predictions of PNM. The successful verification of the developed code allows us conducting forward simulations and predicting the hydraulic and transport properties of PNMs.

The third step in evaluating the pore network modeling result was to determine the sensitivity of the results to the size of time step and the effects of numerical diffusion on the simulation results. The sensitivity of simulation results to the size of time step was studied for diffusional transport and advection-dominant transport cases on the pore network of 2 cm depth peat (Fig. B.3). The figure shows that simulation results are very similar in the runs with different time steps, which means that the results are independent of the sizes of time steps. Numerical diffusion is a matter of concern in the numerical simulation of transport processes and its significance depends on the size of time step. Since in a given PNM simulation study, the

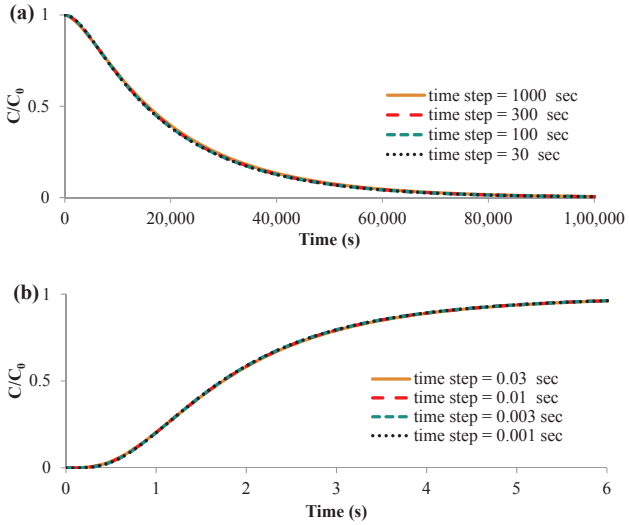

Fig. B.3. (a) variation of solute concentration at $x = L/2$ of peat pore space in a diffusional transport process for peat of 2 cm depth at different time step sizes, (b) variations of effluent solute concentration in an advective-dominant transport process for peat of 2 cm depth at different time step sizes.

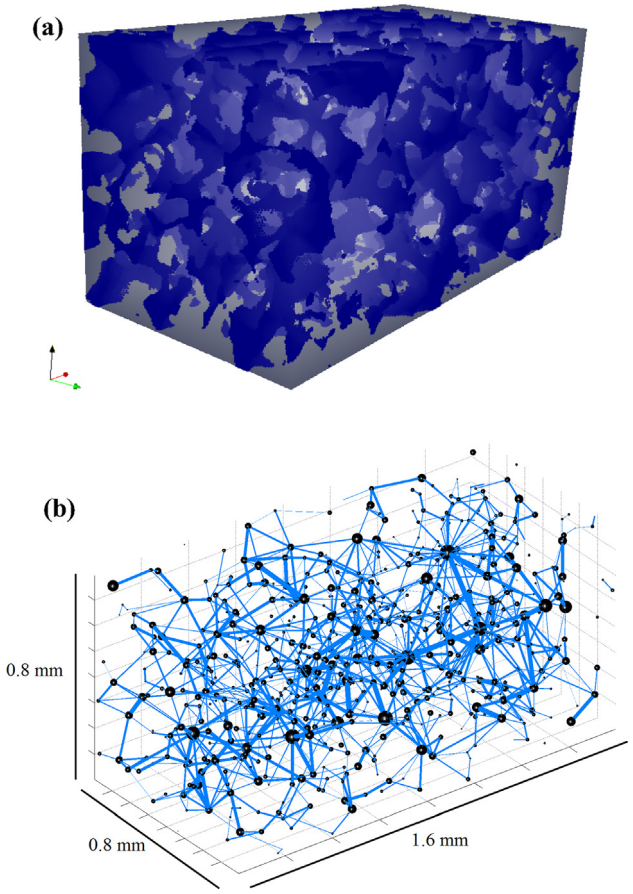

Fig. B.4. (a) CT scan imaging data of Berea sandstone (Imperial College) for sample #1, and (b) the extracted pore network.

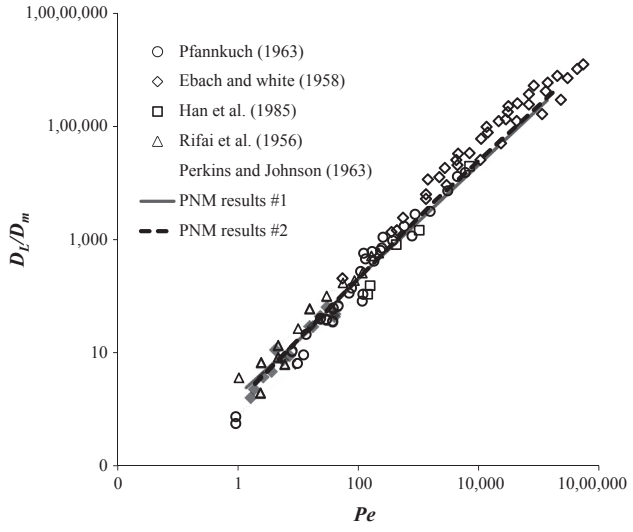

Fig. B.5. Measured D_L/D_m versus Peclet number for granular porous media in comparison to simulated values for Berea sandstone. (See above-mentioned references for further information.)

results do not vary with the size of simulation time step (Fig. B.3) it can be assumed that time step sizes were adequately small to keep the effect of numerical diffusion insignificant compared to the effect of physical transport processes.

The fourth step in validating the pore network modeling code was to compare its results obtained for Berea sandstone to the empirical data available in literature. Bijeljic et al. (2004) constructed PNM using pore data of Berea sandstone, and modeled solute transport at the pore-scale. They compared the calculated D_L/D_m vs. Peclet number (Pe) to the empirical data that were measured for granular porous material and obtained a good agreement between them. A similar evaluation was done in this study. Two subsections (802 μm × 802 μm × 1604 μm) were cut from micro-CT image of Berea sandstone (available in Imperial-College website with resolution of 5.345 μm) (subsection#1 in Fig. B.4a), and the pore network of each was extracted (Fig. B.4b for subsection#1). Then advective-diffusive transport was simulated along each network at different pore water

velocities, and the dispersion coefficient in each simulation was determined by methodology discussed in Appendix C. The calculated D_L/D_m to Pe relations are compared to the empirical data (Fig. B.5). In Fig. B.5, symbols are empirical data of granular media and – excluding Perkins and Johnson (1963) – are reproduced from Han et al. (1985). The grey line and black dashed line are the results of our model, respectively, for subsections #1 and #2. There is a good agreement between our results and the empirical data confirming that our simulation code has a good predictive performance.

Appendix C. Evaluation of bulk hydraulic and transport properties

Hydraulic conductivity

As the simulation of saturated water flow in a pore network ends, Q_w, which is the bulk water flow rate through the pore network [L^3T^{-1}], is calculated using the flow rate of each pore throat (Fig. 3). Using dimensions of pore network and applied upstream and downstream pressures, the equivalent permeability of the pore network is calculated using a form of Darcy's law, given as

$$k_{eq} = \frac{Q_w \mu_w L}{A_{bulk}(P_{upstream} - P_{downstream})} \tag{C.1}$$

where k_{eq} is the equivalent permeability of pore network [L^2], Q_w is bulk water flowing rate [L^3T^{-1}], μ_w is water viscosity [$MT^{-1}L^{-1}$], L is the bulk length of the cube [L], A_{bulk} is bulk cross-sectional area of the soil cube [L^2], and $P_{upstream}$ and $P_{downstream}$ are water pressures [$ML^{-1}T^{-2}$] at the upstream and downstream faces of the network, respectively. The equivalent hydraulic conductivity of the pore network is then calculated by

$$K_{eq} = \frac{k_{eq}\rho_w g}{\mu_w} \tag{C.2}$$

where K_{eq} is equivalent hydraulic conductivity [LT^{-1}], ρ_w is water density [ML^{-3}], and g is acceleration by gravity [LT^{-2}] (Freeze and Cherry, 1979). Horizontal hydraulic conductivity (K_h) and vertical hydraulic conductivity (K_v) of each PNM were determined by applying pressure gradients in the horizontal (e.g. Fig. 2) and vertical directions, respectively.

Hydraulic tortuosity

Depending on the type of traveling particles, the hydraulic tortuosity (τ_h) and diffusional tortuosity (τ_d) are defined for porous media (Clennell, 1997). When fluid particles move through a porous medium the path is tortuous due to the presence of solids, which form flow and transport barriers. The extension of fluid particle movement path necessitates definition of τ_h as

$$\tau_h = \frac{L_{actual}}{L_{apparent}} \tag{C.3}$$

where L_{actual} is the average length of the path that a fluid particle moves through the pore space, and $L_{apparent}$ is the bulk length of porous medium (Bo-Ming and Jian-Hua, 2004; Shen and Chen, 2007).

We obtained the τ_h of peat by tracking fluid particles through PNMs. A number of fluid particles ($N = 10^4$) were placed at the upstream face of the pore network, and the flow path of each particle is tracked until the particle arrives at the downstream face of the network. The average travel path length is calculated as arithmetic mean of the travel length of all the particles. τ_h of pore network is then calculated as the ratio of the average travel length to the bulk length of the network (Fig. C.1).

Diffusional tortuosity and pore shape exponent

Similar to fluids particles, when solute particles move by a diffusional transport, the presence of solids causes the actual path to be longer than bulk length of the porous media. The longer solute travel path in the presence of soil solids reduces the diffusive mass flux and causes the bulk effective diffusion coefficient (D_{eff}) [L^2T^{-1}] to be smaller than the molecular diffusion coefficient (D_m) [L^2T^{-1}] for that solute in water. The relation

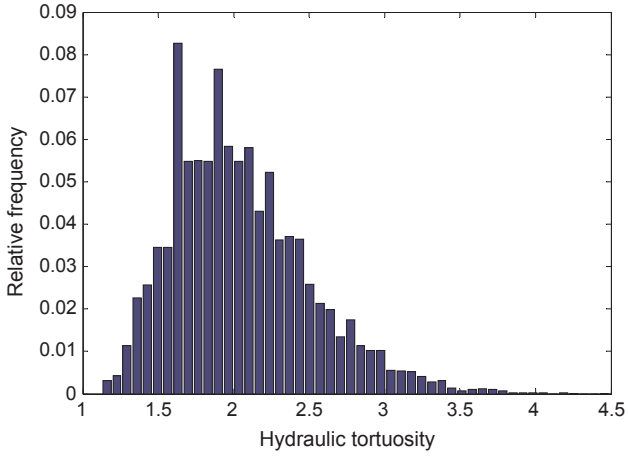

Fig. C.1. Histogram of hydraulic tortuosity of peat PNM at 2 cm depth; the average tortuosity is 2.05 as indicated in Table 1.

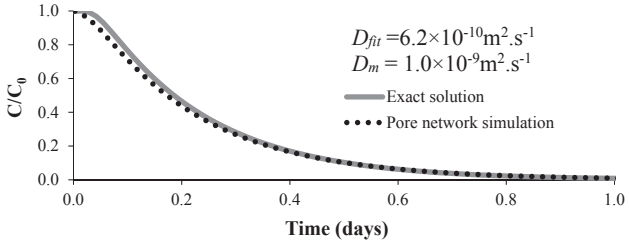

Fig. C.2. Comparison of analytical solution and pore network modeling solution for variation of solute concentration at x = L/2 of a peat cube at 2 cm depth.

between ratios of D_{eff}, D_m, τ_d, and ε of porous media (Moldrup et al., 2001; Gommes et al., 2009) is

$$\tau_d^2 = \frac{D_m}{D_{eff}}\varepsilon \tag{C.4}$$

To calculate D_{eff} of pore networks by network simulations, the water flow rate is assumed to be zero, so the transport process is non-advective. A well-known diffusional transport problem having an exact analytical solution is a cube with length L [L], initial solute concentration of C_o [ML^{-3}], and boundary conditions of $C(0,t) = C(L,t) = 0$. The exact solution for the variation of solute concentration over time and space in the cube is

$$C(x,t) = \frac{4C_0}{\pi}\sum_{i=1}^{\infty}\left[\frac{1}{2i-1}\sin\left(\frac{(2i-1)\pi x}{L}\right)\exp\left(-\frac{(2i-1)^2\pi^2 D_{fit}\,t}{L^2}\right)\right] \tag{C.5}$$

where x is position of observation point [L], D_{fit} is the equivalent diffusion coefficient [L^{2}T^{-1}] of the system, and t is time [T] (Mehrer, 2007). Non-advective solute transport through PNMs is simulated with the same initial condition and the same boundary conditions of the abovementioned problem. To obtain D_{fit} of a pore network, the temporal variation of solute concentration at $x/L = 0.5$ that results from the pore network simulation is compared to that resulting from Eq. (C.5) at $x = L/2$. Then D_{fit} in Eq. (C.5) is adjusted until the solute concentration variation at $x = L/2$ fits the pore network simulation results and the sum of the square of the errors minimizes. Fig. C.2 illustrates an example of pore network simulation results and the fitted exact solution for a peat cube at 2 cm depth. The calculated D_{fit} (5.9×10^{-10} m^{-2}.s^{-1} in Fig. C.2) is around half of D_m (1.0×10^{-9} m^{-2}.s^{-1}) because of the τ_d of peat. Since D_{fit} is back-calculated from the concentration of the solution, it is the effective diffusion coefficient in the aqueous phase. Therefore, D_{eff}, which is the bulk effective diffusion coefficient, is the product of D_{fit} and the porosity. Eventually, diffusional tortuosity, τ_d, can also be calculated using Eq. (C.4) and the calculated D_{eff}.

The formation factor (F) of a porous medium, which is the ratio of electrical conductivity of pure brine to the electrical conductivity of the medium when it is saturated with brine, is inversely correlated with porosity of the porous material by

$$F = \frac{a}{\varepsilon^m} \tag{C.6}$$

where a is a parameter affected by tortuosity, ε is the porosity, and m is the shape (cementation) exponent (Archie, 1942; Winsauer et al., 1952; Liu and Kitanidis, 2013). In this equation, both a and m are empirical parameters and are controlled by pore shape and geometry (Boving and Grathwohl, 2001), and a is different from classic tortuosity (Salem, 1993). Due to the analogy between Ohm's Law as the electrical charge transport equation and Fick's law as the solute transport equation (Klinkenberg, 1951; Liu and Kitanidis, 2013), and considering electrical and diffusional tortuosity (τ_d) are the same (Sahimi, 1994; Clennell, 1997), the formation factor (F) is equal to the ratio of D_m to D_{eff} (Snyder, 2001). Therefore

$$\frac{D_m}{D_{eff}} = a\varepsilon^{-m} \tag{C.7}$$

As corresponding ε of all the PNMs and D_m of the solute are known in solute transport simulations, Eq. (C.7) suggests m and a can be calculated by obtaining D_{eff} of at least two pore networks. After fitting D_{fit} and calculating D_{eff} for the pore networks, τ_d of each network as well as a and m are calculated using Eqs. (C.4) and (C.7).

Dispersivity

Dispersivity is a transport parameter controlling the mixing length between streams of the aqueous phase, such that

$$D_L = \alpha_L v + D_{eff} \tag{C.8}$$

where α_L is longitudinal dispersivity [L], v is average linear flow velocity [LT^{-1}], D_{eff} is effective diffusion coefficient [L^{2}T^{-1}], and D_L is hydrodynamic dispersion [L^{2}T^{-1}] (Appelo and Postma, 2004). Based on this equation, if a set of D_L vs. v data points are available for a porous medium, dispersivity of the medium is calculated as the slope of linear regression. The average linear flow velocity in a porous medium is determined (Appelo and Postma, 2004) as

$$v = \frac{Q_w}{A_{bulk}\,\varepsilon} \tag{C.9}$$

Hydrodynamic dispersion (D_L) and longitudinal dispersivity (α_L) for an advective-diffusive transport process is obtained by analyzing the simulated solute breakthrough curves. In the simulation of unsteady-state solute transport through PNMs, the variation of effluent concentrations with time is the solute breakthrough curve. We fit the simulated solute breakthrough curve with exact solution of Advection Dispersion Equation (Ogata and Banks, 1961) using least-squares method and by considering hydrodynamic dispersion as a tuning parameter to determine the equivalent hydrodynamic dispersion.

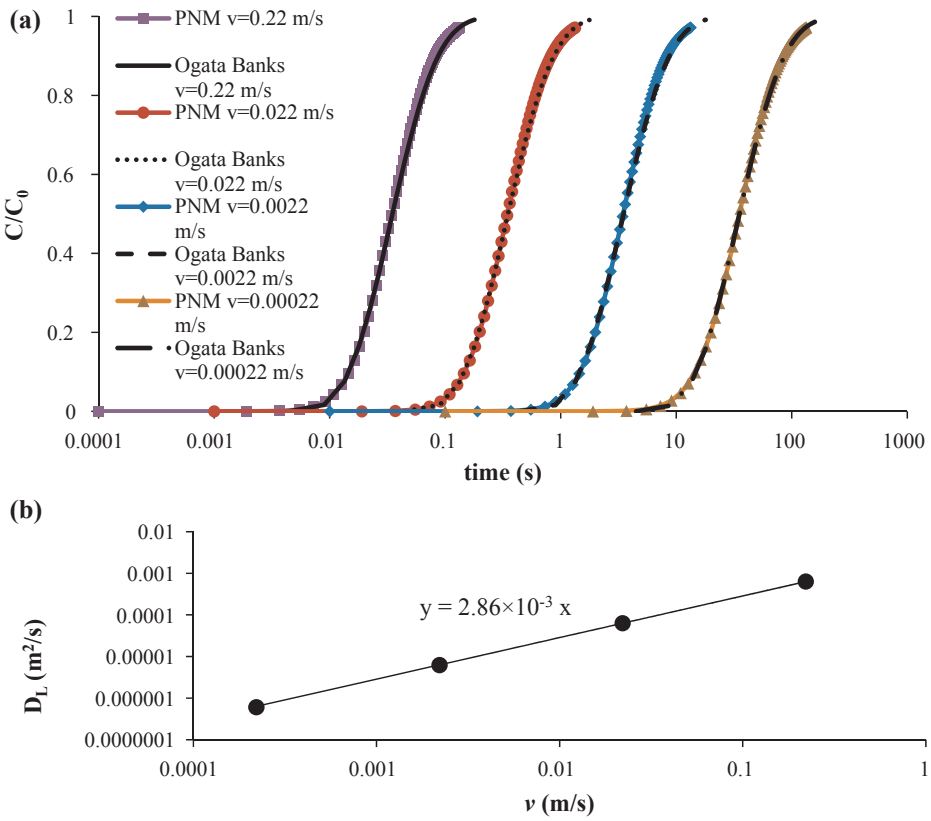

Fig. C.3. (a) Breakthrough curves obtained through pore network simulation and by Ogata-Banks exact solution for the pore network at 2 cm peat depth profile; (b) Variation of hydrodynamic dispersion with average linear flow velocity for the PNM of peat at 2 cm depth.

For PNMs of peat soil, simulating the solute breakthrough curve and fitting it with exact solution are repeated four times in different water velocities (e.g. 0.00022, 0.0022, 0.022, and 0.22 $m.s^{-1}$ in Fig. C.3a), giving the variation of hydrodynamic dispersion with average linear flow velocity. Then, the dispersivity of each PNM is calculated as the slope of D_L vs. v data (e.g. 2.86 mm in Fig. C.3b).

References

Acharya, R.C., Van der Zee, S.E.A.T.M., Leijnse, A., 2005. Transport modeling of non-linearly adsorbing solutes in physically heterogeneous pore networks. Water Resour. Res. 41 (2). http://dx.doi.org/10.1029/2004wr003500.

Acharya, R.C., Van der Zee, S.E.A.T.M., Leijnse, A., 2007. Approaches for modeling longitudinal dispersion in pore-networks. Adv. Water Resour. 30 (2), 261–272. http://dx.doi.org/10.1016/j.advwatres.2005.11.015.

Aghaei, A., Piri, M., 2015. Direct pore-to-core up-scaling of displacement processes: dynamic pore network modeling and experimentation. J. Hydrol. 522, 488–509. http://dx.doi.org/10.1016/j.jhydrol.2015.01.004.

Ahrens, J., Geveci, B., Law, C., 2005. 36-ParaView: an end-user tool for large-data visualization. Visualization Handbook 717–731.

Al-Kharusi, A.S., Blunt, M.J., 2007. Network extraction from sandstone and carbonate pore space images. J. Pet. Sci. Eng. 56 (4), 219–231. http://dx.doi.org/10.1016/j.petrol.2006.09.003.

Al-Raoush, R.I., Willson, C.S., 2005. Extraction of physically realistic pore network properties from three-dimensional synchrotron X-ray microtomography images of unconsolidated porous media systems. J. Hydrol. 300 (1), 44–64. http://dx.doi.org/10.1016/j.jhydrol.2004.05.005.

Appelo, C.A.J., Postma, D., 2004. Geochemistry, Groundwater and Pollution. CRC Press.

Archie, G.E., 1942. The electrical resistivity log as an aid in determining some reservoir characteristics. Trans. AIMe 146 (01), 54–62. http://dx.doi.org/10.2118/942054-g.

Armatas, G.S., 2006. Determination of the effects of the pore size distribution and pore connectivity distribution on the pore tortuosity and diffusive transport in model porous networks. Chem. Eng. Sci. 61 (14), 4662–4675. http://dx.doi.org/10.1016/j.ces.2006.02.036.

Armatas, G.S., Pomonis, P.J., 2004. A Monte Carlo pore network for the simulation of porous characteristics of functionalized silica: pore size distribution, connectivity distribution and mean tortuosities. Chem. Eng. Sci. 59 (24), 5735–5749. http://dx.doi.org/10.1016/j.ces.2004.06.047.

Arns, J.Y., Robins, V., Sheppard, A.P., Sok, R.M., Pinczewski, W.V., Knackstedt, M.A., 2004. Effect of network topology on relative permeability. Transp. Porous Media 55 (1), 21–46. http://dx.doi.org/10.1023/b:tipm.0000007252.68488.43.

Ayachit, U., 2015. The Paraview Guide: a Parallel Visualization Application. Kitware, Incorporated, USA.

Baird, A.J., Gaffney, S.W., 2000. Solute movement in drained fen peat: a field tracer study in a Somerset (UK) wetland. Hydrol. Process. 14 (14), 2489–2503. http://dx.doi.org/10.1002/1099-1085(20001015)14:14<2489::AID-HYP110>3.0.CO;2-Q.

Bear, J., 1972. Dynamics of Fluids in Porous Media. Elsevier, New York.

Beckwith, C.W., Baird, A.J., Heathwaite, A.L., 2003. Anisotropy and depth-related heterogeneity of hydraulic conductivity in a bog peat. II: modelling the effects on groundwater flow. Hydrol. Process. 17 (1), 103–113. http://dx.doi.org/10.1002/hyp.1117.

Berg, S., Rücker, M., Ott, H., Georgiadis, A., van der Linde, H., Enzmann, F., Wiegmann, A., 2016. Connected pathway relative permeability from pore-scale imaging of imbibition. Adv. Water Resour. 90, 24–35. http://dx.doi.org/10.1016/j.advwatres.2016.01.010.

Bijeljic, B., Muggeridge, A.H., Blunt, M.J., 2004. Pore-scale modeling of longitudinal dispersion. Water Resour. Res. 40 (11). http://dx.doi.org/10.1029/2004wr003567.

Bijeljic, B., Blunt, M.J., 2007. Pore-scale modeling of transverse dispersion in porous media. Water Resour. Res. 43 (12). http://dx.doi.org/10.1029/2006wr005700.

Blunt, M.J., 2001. Flow in porous media—pore-network models and multiphase flow. Curr. Opin. Colloid. Interface Sci. 6 (3), 197–207. http://dx.doi.org/10.1016/s1359-0294(01)00084-x.

Blunt, M., King, P., 1991. Relative permeabilities from two-and three-dimensional pore-scale network modelling. Transp. Porous Media 6 (4), 407–433. http://dx.doi.org/10.1007/bf00136349.

Boelter, D.H., Verry, E.S., 1977. Peatland and water in the northern Lake States. In: USDA-Forest Service General Technical Report NC-31, (26pp).

Bo-Ming, Y., Jian-Hua, L., 2004. A geometry model for tortuosity of flow path in porous media. Chin. Phys. Lett. 21 (8), 1569–1571. http://dx.doi.org/10.1088/0256-307x/21/8/044.

Boudreau, J., Caron, J., Elrick, D., Fortin, J., Gallichand, J., 2009. Solute transport in sub-irrigated peat-based growing media. Can. J. Soil Sci. 89 (3), 301–313. http://dx.doi.org/10.4141/CJSS08023.

Boving, T.B., Grathwohl, P., 2001. Tracer diffusion coefficients in sedimentary rocks: correlation to porosity and hydraulic conductivity. J. Contam. Hydrol. 53 (1), 85–100. http://dx.doi.org/10.1016/s0169-7722(01)00138-3.

Carman, P.C., 1937. Fluid flow through granular beds. Trans. Inst. Chem. Eng. 15, 150–166. http://dx.doi.org/10.1016/S0263-8762(97)80003-2.

Chen-Charpentier, B., 1999. Numerical simulation of biofilm growth in porous media. J. Comput. Appl. Math. 103 (1), 55–66. http://dx.doi.org/10.1016/s0377-0427(98)00240-4.
Clennell, M.B., 1997. Tortuosity: a guide through the maze. Geol. Soc. Lond. Spec. Publ. 122 (1), 299–344.
Dong, H., Blunt, M.J., 2009. Pore-network extraction from micro-computerized-tomography images. Phys. Rev. E 80 (3), 036307. http://dx.doi.org/10.1103/physreve.80.036307.
Ebach, E.A., White, R.R., 1958. Mixing of fluids flowing through beds of packed solids. AIChE J. 4 (2), 161–169. http://dx.doi.org/10.1002/aic.690040209.
Ezeuko, C.C., Sen, A., Grigoryan, A., Gates, I.D., 2011. Pore-network modeling of biofilm evolution in porous media. Biotechnol. Bioeng. 108 (10), 2413–2423. http://dx.doi.org/10.1002/bit.23183.
Fetter, C.W., 1999. Contaminant hydrogeology. Prentice hall, New Jersey.
Fraser, C.J.D., Roulet, N.T., Lafleur, M., 2001. Groundwater flow patterns in a large peatland. J. Hydrol. 246 (1), 142–154. http://dx.doi.org/10.1016/s0022-1694(01)00362-6.
Freeze, R.A., Cherry, J.A., 1979. Groundwater. Prentice-Hall Inc, Englewood Cliffs, New Jersey.
Ghanbarian, B., Hunt, A.G., Ewing, R.P., Sahimi, M., 2013. Tortuosity in porous media: a critical review. Soil Sci. Soc. Am. J. 77 (5), 1461–1477. http://dx.doi.org/10.2136/sssaj2012.0435.
Gommes, C.J., Bons, A.J., Blacher, S., Dunsmuir, J.H., Tsou, A.H., 2009. Practical methods for measuring the tortuosity of porous materials from binary or gray-tone tomographic reconstructions. AIChE J. 55 (8), 2000–2012. http://dx.doi.org/10.1002/aic.11812.
Han, N.W., Bhakta, J., Carbonell, R.G., 1985. Longitudinal and lateral dispersion in packed beds: effect of column length and particle size distribution. AIChE J. 31 (2), 277–288. http://dx.doi.org/10.1002/aic.690310215.
Hoag, R.S., Price, J.S., 1995. A field-scale, natural gradient solute transport experiment in peat at a Newfoundland blanket bog. J. Hydrol. 172 (1), 171–184. http://dx.doi.org/10.1016/0022-1694(95)02696-m.
Hoag, R.S., Price, J.S., 1997. The effects of matrix diffusion on solute transport and retardation in undisturbed peat in laboratory columns. J. Contam. Hydrol. 28 (3), 193–205. http://dx.doi.org/10.1016/s0169-7722(96)00085-x.
Imperial-College (Berea sandstone), http://www.imperial.ac.uk/earth-science/research/research-groups/perm/research/pore-scale-modelling/micro-ct-images-and-networks/berea-sandstone. Retrieved 4/4/2018.
Kantak, M.V., Shetty, S.A., Kelkar, B.G., 1994. Liquid phase backmixing in bubble column reactors—a new correlation. Chem. Eng. Commun. 127 (1), 23–34. http://dx.doi.org/10.1080/00986449408936223.
Kim, D., Peters, C.A., Lindquist, W.B., 2011. Upscaling geochemical reaction rates accompanying acidic CO2-saturated brine flow in sandstone aquifers. Water Resour. Res. 47 (1). http://dx.doi.org/10.1029/2010wr009472.
Klinkenberg, L.J., 1951. Analogy between diffusion and electrical conductivity in porous rocks. Geol. Soc. Am. Bull. 62 (6), 559–564. http://dx.doi.org/10.1130/0016-7606(1951) 62[559:ABDAEC]2.0.CO;2.
Klotz, D., Seiler, K.P., Moser, H., Neumaier, F., 1980. Dispersivity and velocity relationship from laboratory and field experiments. J. Hydrol. 45 (3–4), 169–184. http://dx.doi.org/10.1016/0022-1694(80)90018-9.
Köhne, J.M., Schlüter, S., Vogel, H.J., 2011. Predicting solute transport in structured soil using pore network models. Vadose Zone J. 10 (3), 1082–1096. http://dx.doi.org/10.2136/vzj2010.0158.
Kruse, J., Lennartz, B., Leinweber, P., 2008. A modified method for measuring saturated hydraulic conductivity and anisotropy of fen peat samples. Wetlands 28 (2), 527–531. http://dx.doi.org/10.1672/07-153.1.
Lewis, C., Albertson, J., Xu, X., Kiely, G., 2012. Spatial variability of hydraulic conductivity and bulk density along a blanket peatland hillslope. Hydrol. Process. 26 (10), 1527–1537. http://dx.doi.org/10.1002/hyp.8252.
Li, L., Peters, C.A., Celia, M.A., 2006. Upscaling geochemical reaction rates using pore-scale network modeling. Adv. Water Resour. 29 (9), 1351–1370. http://dx.doi.org/10.1016/j.advwatres.2005.10.011.
Liu, Y., Kitanidis, P.K., 2013. Tortuosity and Archie's law. In: Advances in Hydrogeology. Springer, New York, pp. 115–126. http://dx.doi.org/10.1007/978-1-4614-6479-2_6.
McCarter, C.P.R., Price, J.S., 2017a. Experimental hydrological forcing to illustrate water flow processes of a subarctic ladder fen peatland. Hydrol. Process. 31 (8), 1578–1589. http://dx.doi.org/10.1002/hyp.11127.
McCarter, C.P.R., Price, J.S., 2017b. The transport dynamics of chloride and sodium in a ladder fen during a continuous wastewater polishing experiment. J. Hydrol. 549, 558–570. http://dx.doi.org/10.1016/j.jhydrol.2017.04.033.
Mehmani, Y., Balhoff, M.T., 2015. Eulerian network modeling of longitudinal dispersion. Water Resour. Res. 51 (10), 8586–8606. http://dx.doi.org/10.1002/2015wr017543.
Mehmani, Y., Oostrom, M., Balhoff, M.T., 2014. A streamline splitting pore-network approach for computationally inexpensive and accurate simulation of transport in porous media. Water Resour. Res. 50 (3), 2488–2517. http://dx.doi.org/10.1002/2013wr014984.
Mehmani, Y., Tchelepi, H.A., 2017. Minimum requirements for predictive pore-network modeling of solute transport in micromodels. Adv. Water Resour. 108, 83–98. http://dx.doi.org/10.1016/j.advwatres.2017.07.014.
Mehrer, H., 2007. Diffusion in solids: fundamentals, methods, materials, diffusion-controlled processes. Springer Science Business Media.
Meyers, J.J., Liapis, A.I., 1998. Network modeling of the intraparticle convection and diffusion of molecules in porous particles packed in a chromatographic column. J. Chromatogr. A 827 (2), 197–213. http://dx.doi.org/10.1016/s0021-9673(98)00658-x.
Meyers, J.J., Liapis, A.I., 1999. Network modeling of the convective flow and diffusion of molecules adsorbing in monoliths and in porous particles packed in a chromatographic column. J. Chromatogr. A 852 (1), 3–23. http://dx.doi.org/10.1016/s0021-9673(99)00443-4.
MICROVIEW, Parallax Innovations, www.parallax-innovations.com/microview.html.
Moldrup, P., Olesen, T., Komatsu, T., Schjønning, P., Rolston, D.E., 2001. Tortuosity, diffusivity, and permeability in the soil liquid and gaseous phases. Soil Sci. Soc. Am. J. 65 (3), 613–623. http://dx.doi.org/10.2136/sssaj2001.653613x.
Mostaghimi, P., Blunt, M.J., Bijeljic, B., 2013. Computations of absolute permeability on micro-CT images. Math. Geosci. 45 (1), 103–125. http://dx.doi.org/10.1007/s11004-012-9431-4.
Nordhaug, H.F., Celia, M., Dahle, H.K., 2003. A pore network model for calculation of interfacial velocities. Adv. Water Resour. 26 (10), 1061–1074. http://dx.doi.org/10.1016/s0309-1708(03)00100-3.
Ogata, A., Banks, R. B., 1961. A solution of the differential equation of longitudinal dispersion in porous media, Geological Survey Professional Paper 411-A, United States.
OpenFOAM, The open source CFD toolbox, www.openfoam.com.
Oren, P.E., Bakke, S., Arntzen, O.J., 1998. Extending predictive capabilities to network models. SPE J. 3 (04), 324–336. http://dx.doi.org/10.2118/52052-pa. 10.2118/52052-PA.
Ours, D.P., Siegel, D.I., Glaser, P.H., 1997. Chemical dilation and the dual porosity of humified bog peat. J. Hydrol. 196 (1), 348–360. http://dx.doi.org/10.1016/s0022-1694(96)03247-7.
Perkins, T.K., Johnston, O.C., 1963. A review of diffusion and dispersion in porous media. Soc. Pet. Eng. J. 3 (01), 70–84. http://dx.doi.org/10.2118/480-PA.
Pfannkuch, H.O., 1963. Contribution a l' etude des deplacements defluiedes miscibles dans un milieu poreux. Rev. Inst. Fr. Pet. 18, 215–270.
Price, J.S., Whittington, P.N., Elrick, D.E., Strack, M., Brunet, N., Faux, E., 2008. A method to determine unsaturated hydraulic conductivity in living and undecomposed moss. Soil Sci. Soc. Am. J. 72 (2), 487–491. http://dx.doi.org/10.2136/sssaj2007.0111n.
Qin, C.Z., Hassanizadeh, S.M., 2015. Pore-network modeling of solute transport and biofilm growth in porous media. Transp. Porous Media 110 (3), 345–367. http://dx.doi.org/10.1007/s11242-015-0546-1.
Quinton, W.L., Hayashi, M., Carey, S.K., 2008. Peat hydraulic conductivity in cold regions and its relation to pore size and geometry. Hydrol. Process. 22 (15), 2829–2837. http://dx.doi.org/10.1002/hyp.7027.
Quinton, W.L., Elliot, T., Price, J.S., Rezanezhad, F., Heck, R., 2009. Measuring physical and hydraulic properties of peat from X-ray tomography. Geoderma 153 (1), 269–277. http://dx.doi.org/10.1016/j.geoderma.2009.08.010.
Raoof, A., Hassanizadeh, S., Leijnse, A., 2010. Upscaling transport of adsorbing solutes in porous media: pore-network modeling. Vadose Zone J. 9 (3), 624. http://dx.doi.org/10.2136/vzj2010.0026.
Raoof, A., Nick, H.M., Hassanizadeh, S.M., Spiers, C.J., 2013. PoreFlow: a complex pore-network model for simulation of reactive transport in variably saturated porous media. Comput. Geosci. 61, 160–174. http://dx.doi.org/10.1016/j.cageo.2013.08.005.
Rezanezhad, F., Quinton, W.L., Price, J.S., Elrick, D., Elliot, T.R., Heck, R.J., 2009. Examining the effect of pore size distribution and shape on flowthrough unsaturated peat using computed tomography. Hydrol. Earth Syst. Sci. 13, 1993–2002. http://dx.doi.org/10.5194/hessd-6-3835-2009.
Rezanezhad, F., Quinton, W.L., Price, J.S., Elliot, T.R., Elrick, D., Shook, K.R., 2010. Influence of pore size and geometry on peat unsaturated hydraulic conductivity computed from 3D computed tomography image analysis. Hydrol. Process. 24 (21), 2983–2994. http://dx.doi.org/10.1002/hyp.7709.
Rezanezhad, F., Price, J.S., Craig, J.R., 2012. The effects of dual porosity on transport and retardation in peat: A laboratory experiment. Can. J. Soil Sci. 92 (5), 723–732. http://dx.doi.org/10.4141/cjss2011-050.
Rifai, M.N.E., Kaufman, W.J., Todd, D.K., 1956. Dispersion Phenomena in Laminar Flow Through Porous Media. University of California, Sanitary Engineering Research Laboratory and Division of Civil Engineering.
Rosa, E., Larocque, M., 2008. Investigating peat hydrological properties using field and laboratory methods: application to the Lanoraie peatland complex (southern Quebec, Canada). Hydrol. Process. 22 (12), 1866–1875. http://dx.doi.org/10.1002/hyp.6771.
Sahimi, M., 1994. Applications of Percolation Theory. CRC Press.
Salem, H.S., 1993. Derivation of the cementation factor (Archie's Exponent) and the Kozeny–Carmen constant from well log data, and their dependence on lithology and other physical parameters. paper SPE 26309 available from SPE, Richardson, Texas.
Salem, H.S., 2001. Determination of porosity, formation resistivity factor, Archie cementation factor, and pore geometry factor for a glacial aquifer. Energy Sources 23 (6), 589–596. http://dx.doi.org/10.1080/00908310152125238.
Saomoto, H., Katagiri, J., 2015. Direct comparison of hydraulic tortuosity and electric tortuosity based on finite element analysis. Theor. Appl. Mech. Lett. 5 (5), 177–180. http://dx.doi.org/10.1016/j.taml.2015.07.001.
Sharratt, P.N., Mann, R., 1987. Some observations on the variation of tortuosity with Thiele modulus and pore size distribution. Chem. Eng. Sci. 42 (7), 1565–1576. http://dx.doi.org/10.1016/0009-2509(87)80161-6.
Shen, L., Chen, Z., 2007. Critical review of the impact of tortuosity on diffusion. Chem. Eng. Sci. 62 (14), 3748–3755. http://dx.doi.org/10.1016/j.ces.2007.03.041.
Sheng, Q., Thompson, K., 2016. A unified pore-network algorithm for dynamic two-phase flow. Adv. Water Resour. 95, 92–108. http://dx.doi.org/10.1016/j.advwatres.2015.12.010.
Silin, D., Patzek, T., 2006. Pore space morphology analysis using maximal inscribed spheres. Phys. A 371 (2), 336–360. http://dx.doi.org/10.1016/j.physa.2006.04.048.
Snyder, K.A., 2001. The relationship between the formation factor and the diffusion coefficient of porous materials saturated with concentrated electrolytes: theoretical

and experimental considerations. Concr. Sci. Eng. 3 (12), 216–224.
Suchomel, B.J., Chen, B.M., Allen, M.B., 1998a. Network model of flow, transport and biofilm effects in porous media. Transp. Porous Media 30 (1), 1–23. http://dx.doi.org/10.1023/A:1006560705680.
Suchomel, B.J., Chen, B.M., Allen, M.B., 1998b. Macroscale properties of porous media from a network model of biofilm processes. Transp. Porous Media 31 (1), 39–66. http://dx.doi.org/10.1023/A:1006506104835.
Thullner, M., Baveye, P., 2008. Computational pore network modeling of the influence of biofilm permeability on bioclogging in porous media. Biotech. Bioeng. 99 (6), 1337–1351. http://dx.doi.org/10.1002/bit.21708.
Valvatne, P.H., Blunt, M.J., 2004. Predictive pore-scale modeling of two-phase flow in mixed wet media. Water Resour. Res. 40 (7). http://dx.doi.org/10.1029/2003wr002627.
Vogel, H.J., 2000. A numerical experiment on pore size, pore connectivity, water retention, permeability, and solute transport using network models. Eur. J. Soil Sci. 51 (1), 99–105. http://dx.doi.org/10.1046/j.1365-2389.2000.00275.x.
Vogel, H.J., Roth, K., 1998. A new approach for determining effective soil hydraulic functions. Eur. J. Soil Sci. 49 (4), 547–556. http://dx.doi.org/10.1046/j.1365-2389.1998.4940547.x.
Vogel, H.J., Roth, K., 2001. Quantitative morphology and network representation of soil pore structure. Adv. Water Resour. 24 (3), 233–242. http://dx.doi.org/10.1016/s0309-1708(00)00055-5.
Vogel, H.J., 2002. Topological characterization of porous media. In: Morphology of Condensed Matter. Springer, Berlin Heidelberg, pp. 75–92. http://dx.doi.org/10.1007/3-540-45782-8_3.
Winsauer, W.O., Shearin Jr, H.M., Masson, P.H., Williams, M., 1952. Resistivity of brine-saturated sands in relation to pore geometry. AAPG Bull. 36 (2), 253–277. http://dx.doi.org/10.1306/3d9343f4-16b1-11d7-8645000102c1865d.
Wyble, D.O., 1958. Effect of applied pressure on the conductivity, porosity and permeability of sandstones. J. Pet. Technol. 10 (11), 57–59. http://dx.doi.org/10.2118/1081-g.
Yiotis, A.G., Stubos, A.K., Boudouvis, A.G., Yortsos, Y.C., 2001. A 2-D pore-network model of the drying of single-component liquids in porous media. Adv. Water Resour. 24 (3), 439–460. http://dx.doi.org/10.1016/s0309-1708(00)00066-x.
Zhang, X., Knackstedt, M.A., 1995. Direct simulation of electrical and hydraulic tortuosity in porous solids. Geophys. Res. Lett. 22 (17), 2333–2336. http://dx.doi.org/10.1029/95gl02230.